

A Novel Charging Methodology for Enhancing the Reliability of Solar Gel Batteries in Renewable Energy Systems

Raja Yahmadi ¹, and Kais Brik ^{2,*}

^{1,2*} University of Carthage, National Institute of Applied Science and Technology, Research Laboratory Materials, Measurements and Applications, Tunis, Tunisia

^{2*} University of Manouba, Higher Institute of Multimedia Arts of Manouba, Manouba, Tunisia

yahmadiraja@gmail.com, kais.brik@yahoo.fr

Abstract

Solar gel batteries are widely used in Renewable Energy (RE) systems. However, harsh climatic and operational conditions pose major challenges in terms of reliability, safety, and performance. Improving battery reliability and performance requires a detailed understanding of the physical, electrochemical, and chemical processes occurring during charging and discharging cycles. In this study, the aging mechanisms of solar gel batteries are analyzed using Failure Mode and Effects Analysis (FMEA) to identify critical failure modes and their causes. Common charging profiles, including Constant Current (CC), Constant Voltage (CV), Constant Current-Constant Voltage CC-CV, Constant Current-Constant Voltage-Constant Current CC-CV-CC, and Pulse Current (PC), are first analyzed based on the battery voltage response to assess their influence on performance and charging time. A fuzzy logic-based approach is used to compute the Fuzzy Risk Priority Number (FRPN) using Occurrence (O), Severity (S), and Non-detection (ND) as input parameters. The charging profiles are then evaluated by combining the reliability factor (FRPN) and charging time using multi-criteria methods, including the combined score, TOPSIS, and Pareto analysis. The CC-CV-CC profile shows the best compromise among the conventional profiles with a Combined score of 0.465 and a TOPSIS score of 0.986. In addition, a new charging profile derived from PC and CC-CV-CC is proposed to mitigate aging mechanisms while optimizing charging time, achieving the highest TOPSIS score (0.988) and lying on the Pareto front. The results demonstrate an improved balance between charging efficiency and battery reliability for RE systems.

Index-words: Battery Degradation, Charging Profiles, Failure Mode and Effect Analysis, Fuzzy Logic Method, Multi-criteria Decision Analysis, Solar Gel Battery.

I. Introduction

In most RE applications, energy storage systems, especially batteries, are employed to ensure energy supply due to their low cost and availability in the marketplace. Despite the advancements made recently in the field of batteries, their performance is still characterized by deterioration over time due to the severe environments and operating conditions such as high temperature, overcharging, incomplete charge, and deep discharging [1-3]. These factors negatively affect the battery's physical, chemical, and electrochemical behavior, thereby accelerating the emergence of different aging modes and their interactions [4-6]. As a result, lead-acid batteries emerge as the most fragile components of the system, with a significant economic impact related to the replacement of the defective batteries.

Focusing on early intervention and prevention is necessary to address this issue. This can be achieved by optimizing battery design parameters and manufacturing processes or by minimizing the occurrence of aging modes during operation in RE applications. The proposed approach in this article focuses on minimizing aging mechanisms and limiting their effects during operation through a suitable choice of charge profile. The most common charge profiles are Constant Current (CC), Constant Voltage (CV), Constant Current-Constant Voltage (CC-CV), Constant Current-Constant Voltage-Constant Current (CC-CV-CC), and Pulse Current (PC) [7-9]. Such charging profiles typically induce increased current stress during the early charging stage, higher operating voltages, prolonged charging durations, and enhanced thermal effects. Many research works have focused on the advantages

* Corresponding author

and disadvantages of the various charge profiles. Hamed Bizhani et al [9] give a comparison of several lead-acid battery charging profiles based on electro-thermal performance factors, such as charging time, temperature, and battery voltage. Melvyn James et al [10] applied a pulse charge profile to submarine lead-acid batteries. According to the preliminary test findings, the pulse profile enhances the battery charge levels and reduces gas evolution rates. Sandhya Lavety et al [11] conducted a comparative assessment of temperature-controlled and uncontrolled charging strategies aimed at enhancing battery longevity and reducing charging duration. The study shows that a pulse-based charging strategy incorporating thermal control reduces the charging time by approximately 60% compared with the CC-CV protocol. Other studies have reported that the high-frequency impulse profiles are not superior to the CC-CV profile [9, 12]. Hybrid optimization and interpretable machine learning approaches have recently proven effective for improving renewable-powered grid performance and stability [13, 14]. In this context, choosing a suitable charging profile for the battery, specifically in RE applications, is challenging and remains an active research area that necessitates a thorough investigation.

Many factors must be considered when choosing the charge profile, such as the charging rate, charging time, and charging method. Battery charging in RE applications is controlled by cell properties and the energy source's output power. High-rate charging may induce thermal stress and deterioration of the active components in the electrodes, leading to a shorter operational life. However, slowly charging (with a low rate) can extend the time it takes to charge and may not fully charge the battery, which could reduce its overall capacity [4, 15]. This is particularly important in RE applications, where weather conditions such as cloudy or rainy days can further limit the available power and influence the choice of an optimal charging profile. Extended durations required for charging, therefore, represent a major challenge for the integration of batteries in RE applications, potentially increasing costs due to the need for expanded battery arrays or specialized charging equipment. For that, it is crucial to consider the charging time when selecting a charge profile to ensure system efficiency, reliability, and cost-effectiveness.

In addition to these factors, the battery's age and temperature should be considered when choosing the charge profile in RE applications. Batteries

subjected to high temperatures or increased aging may require tailored charging profiles to maintain optimal performance and ensure safety.

Overall, an in-depth study of the impact of different charge profiles on batteries is important for ensuring optimal performance, lifetime, and safety. This study applies a Fuzzy approach to evaluate the effects of various charge currents on battery reliability in RE applications, taking into account the charging duration, charge rate, temperature, and battery age. Failures are assessed using a Risk Priority Number (RPN) derived from severity (S), Occurrence (O), and Non-detection (ND) [16], which allows identification and prioritization of critical failure modes. Traditional FMECA can be limited due to the difficulty in precisely assigning these values and the equal weighting of all factors [17, 18]. To address these challenges, fuzzy FMEA is employed [19-21], using linguistic variables and membership functions to handle uncertainty, improve the objectivity of risk assessment, and provide a more realistic evaluation of battery degradation. Building on this, the FRPN is used to quantify the reliability of each profile, and a multi-criteria analysis combining FRPN and charging time is applied to compare them. This approach not only identifies the most suitable charge strategy for RE applications but also provides a systematic and quantitative framework for evaluating and optimizing charge profiles, advancing beyond the limitations of previous methods.

The rest of this paper outlines a structured approach for enhancing battery reliability in RE applications, with Section 2 providing a detailed description of the proposed analysis method. Section 3 provides an overview of the aging mechanisms of solar gel batteries and their causes using the FMEA method. Section 4 evaluates the impact of various charging profiles on battery performance and reliability. This section begins with an overview of the most commonly employed charging profiles in RE systems, then computes the FRPN using a fuzzy logic-based approach. At the end of this section, a multi-criteria analysis based on the combined score, TOPSIS ranking, and Pareto analysis is applied to identify the most suitable charging strategy in terms of reliability and charging duration. Section 5 proposes a novel reliability-oriented charging methodology that integrates the advantages of specific charging profiles to mitigate aging mechanisms while optimizing charging performance, and evaluates it using the same multi-criteria analysis. Finally, in section 6, some conclusions are presented.

II. Methodological framework

The overall methodological framework developed in this study to assess and optimize charging current profiles for solar gel batteries used in RE applications is illustrated in Figure 1. Degradation analysis, FMEA approach, and fuzzy logic theory are all integrated into the proposed methodology to quantitatively assess the impact of various charging strategies on battery aging and operational performance. The framework also incorporates multi-criteria evaluation to ensure a comprehensive assessment of charging strategies in terms of reliability factor and charging time.

The process begins with a comprehensive review of aging phenomena affecting solar gel batteries, including electrode corrosion, hard sulfation of the electrodes, electrolyte stratification, and loss of active material. For each degradation mode, the corresponding causes and effects on battery performance are analyzed and organized using the FME structure. The results of this stage provide the fundamental knowledge required to assess the risks associated with different charging conditions.

The second stage involves a detailed investigation of the charging current profiles used in RE applications to understand their influence on battery performance and degradation. The evaluation is considered using an electrical equivalent circuit model that captures the physicochemical, chemical, and electrochemical behavior of the battery. Different charging profiles are applied under controlled simulation conditions, where key operational parameters such as charging time, charging current rate, and battery voltage behavior during charging are analyzed. These parameters directly influence the severity and occurrence of the degradation mechanisms identified in the previous stage. Consequently, they serve as the basis for evaluating the risk factors within the FMEA framework.

In the third stage, a fuzzy logic-based FMEA approach is implemented to address the limitations of conventional FMEA methods, particularly in dealing with uncertainty and imprecision inherent in risk evaluation. The FMEA risk factors S, O, and ND are used as input variables of the fuzzy

inference system. Each variable is represented by appropriate linguistic membership functions that reflect expert knowledge and the uncertainty associated with battery degradation processes. A set of fuzzy inference rules in the form of 'if-Then' statements is defined to describe the relationship between the input risk factors and the resulting risk level. The fuzzy inference process is performed using the Mamdani approach with min-max inference operations. The aggregated fuzzy output is then transformed into a numerical value representing the FRPN through the center of gravity defuzzification method [22-29].

In the fourth stage, the calculated FRPN values are used to evaluate and compare the degradation risk associated with each charging current profile. The total FRPN provides a quantitative indicator of the potential impact of each charging strategy on battery reliability and lifetime. In addition to the degradation risk assessment, the charging time factor is also considered to ensure that the evaluation reflects both battery durability and operational efficiency requirements. Based on these criteria, a comprehensive comparison of the different charging profiles is performed using multi-criteria decision-making methods, including Combined score evaluation, TOPSIS ranking, and Pareto analysis. This approach enables the identification of the most suitable charging strategy by considering the trade-off between reliability and charging performance in RE systems.

Finally, an optimized charging current profile is proposed to balance fast charging capability with battery longevity. The strategy considers electrochemical behavior and operational constraints, as well as manufacturer charging recommendations, to ensure safe and efficient system operation while enhancing durability. It integrates the results of the degradation analysis, the fuzzy FMEA-based FRPN evaluation, and the multi-criteria decision-making results, including the combined score, TOPSIS ranking, and Pareto analysis, to compare the proposed profile with conventional strategies. This allows the identification of the most effective charging strategy and highlights the advantages of the new profile in a systematic and quantitative manner.

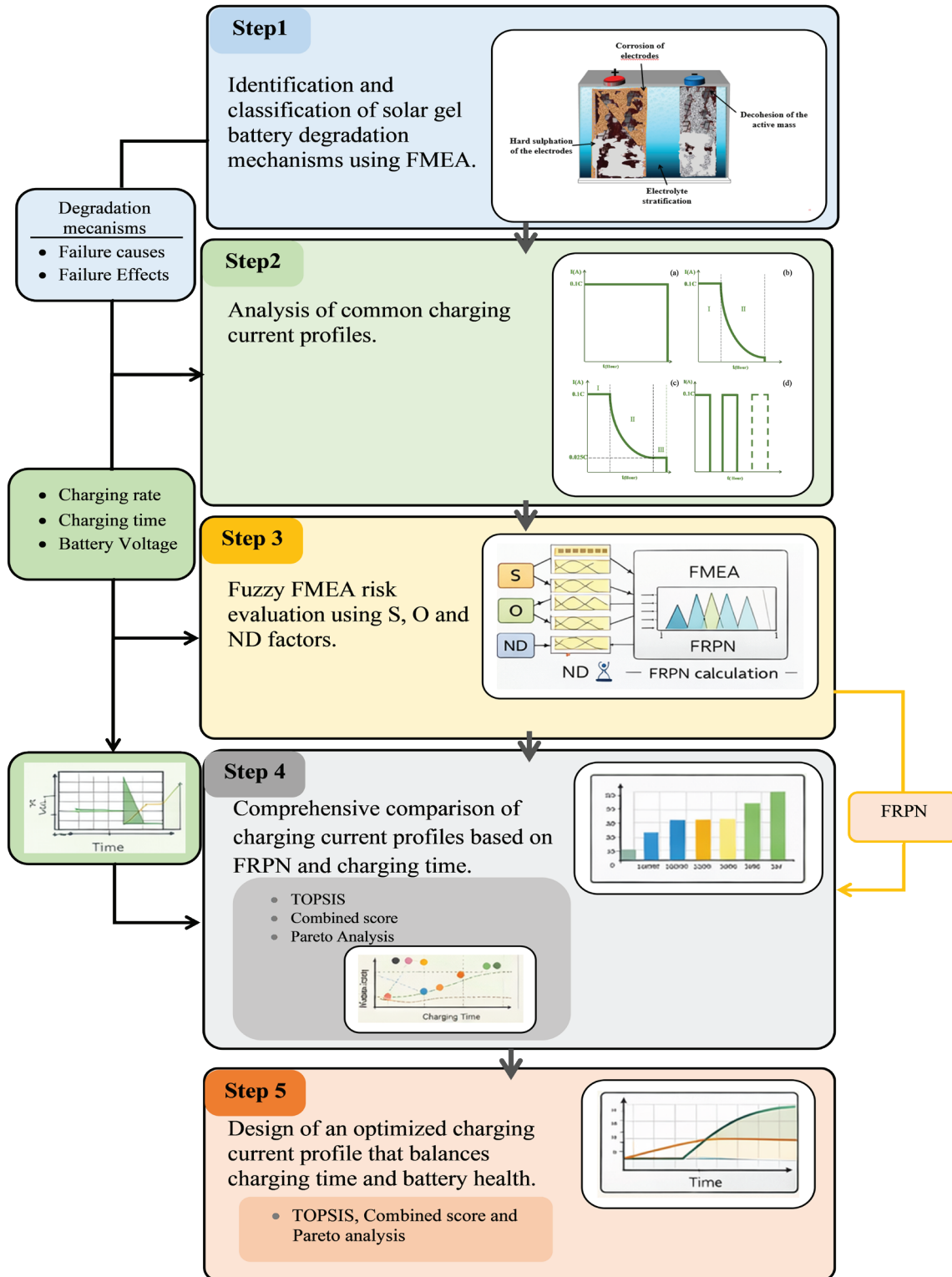


Figure 1: Methodological workflow for evaluating and optimizing charging current profiles for solar gel batteries.

III. Aging mechanisms of the solar battery

The variability of energy supply and improper charging strategies can induce harmful chemical, physico-chemical, and electrochemical reactions on

the different components of the battery [22]. The battery experiences multiple aging processes, with the electrodes subjected to active mass detachment, hard sulfation, and corrosion phenomena, and the electrolyte affected primarily by stratification, as illustrated in Figure 2.

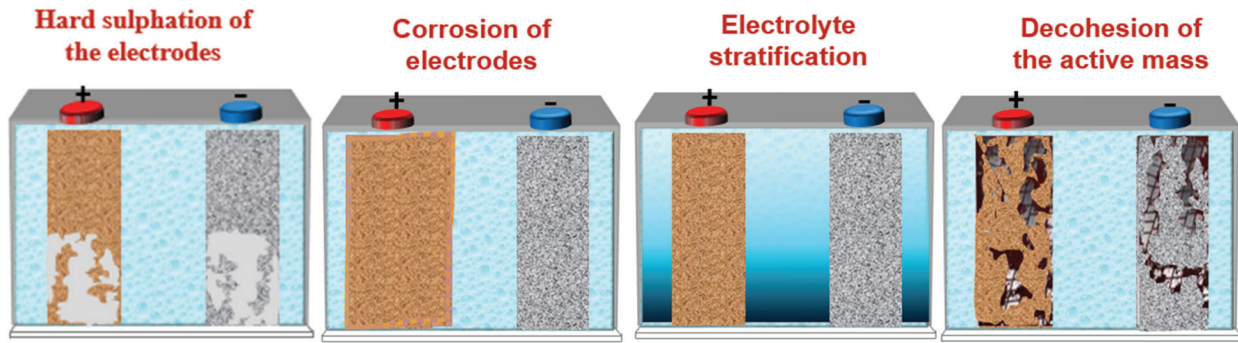


Figure 2: Aging modes of solar batteries.

Table 1: FMEA of solar gel battery

The decohesion of the active mass is characterized by active mass degradation and shedding. Over time, the active mass on the battery plates degrades and changes its structure, cohesion, PbO₂ distribution, and size. It loses some electrical transfer properties and reduces the battery capacity [8]. The shedding occurs when the active material separates from the electrode structure, causing particles to collect at the cell bottom and can trigger internal short circuits between the positive and negative electrodes [5]. It is due to bad operation of the charger, a high temperature, a deep discharge, intensive use: fast charging and discharging, or an overcharge.

Electrode corrosion occurs when insufficient electrolyte coverage exposes the electrode surface, leading to oxidation [7]. This degradation increases internal resistance and reduces capacity, and is accelerated by high temperature, improper charging, intensive use: fast charging and discharging, and an overcharge.

Hard sulfation occurs when electrodes remain deeply discharged for extended periods, leading to the growth of lead sulfate (PbSO₄) crystals that are difficult to dissolve during subsequent charge. As a result, an electrical insulating layer is created, and the amount of the active mass decreases.

Electrolyte stratification, resulting from acid accumulation at the cell bottom, induces localized electrode reactions and diminishes the overall battery capacity. Incomplete charge and deep discharge contribute to electrolyte stratification. To improve battery reliability and durability in RE applications, an FMEA-based assessment is performed to identify key causes and contributors to degradation affecting both the electrode and electrolyte (Table 1).

Function	Failure modes	Effects	Causes
The ability of the battery to supply the voltage and current necessary to supply a load.	F1: Stratification of electrolyte	<ul style="list-style-type: none"> - Acid accumulation at the cell bottom. - An inhomogeneity of the electrodes' discharge. - Capacity fade. 	C1: Deep discharge and absence of charge C2: Cycling with an incomplete charge
	F2: Corrosion of the electrodes	<ul style="list-style-type: none"> - Contact loss with electrolyte - Oxidation of lead grid to PbO₂. - Mechanical weakening of the grid due to lead consumption, Pb. 	C3: Bad operation of the charger
			C4: Overcharge
			C5: High temperature
F3: Hard sulfating of the electrodes	<ul style="list-style-type: none"> - Formation of an electrically insulating layer, a low porosity layer limiting acid diffusion. 	C1: Deep discharge and absence of charge C2: Cycling with an incomplete charge	
F4: Poor cohesion of the active mass	<ul style="list-style-type: none"> - Shedding: Change of the active mass structure - Degradation of the active mass with particles shedding at the cell bottom. 		C3: Bad operation of the charger
			C5: High temperature
			C4: Overcharge
			C1: Deep discharge and absence of charge
			C6: Intensive use: fast charging and discharging
			C7: Cycling

IV. Overview of charging profiles' impact on the battery performance and reliability

A. Equivalent electric circuit model

In many research studies, the evaluation of the efficacy of various charge profiles was based on the battery model [9, 11]. The battery can be modeled by: the mathematical model, the electrical model, and the

electrochemical model [30]. Among these models, the electric equivalent circuit model is the most suitable, which can take into account the chemical, physicochemical, and electrochemical phenomena acting during the charging and discharging modes. It also allows for easy simulation of the battery behavior in real-time, such as state of charge (SOC), terminal voltage, current, internal resistance, etc [11, 31]. An equivalent electric circuit model of a battery is shown in Fig.3.

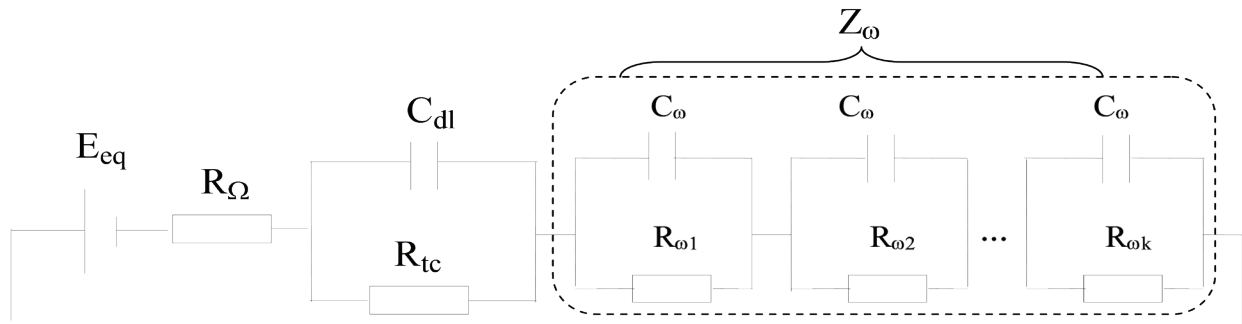


Figure 3: Electrical equivalent circuit.

Where the internal resistance R_{Ω} represents the voltage drop in the electrolyte and electrodes. Both the double-layer capacitance C_{dl} and the charge transfer resistance R_{tc} model the charge transfer zone. Z_w is the Warburg impedance, which is an infinite sum of parallel RC cells representing the diffusion phenomenon [32].

The SOC can be calculated by the current integration method [33].

$$SOC(t) = SOC_{ini} + \frac{\int i_{bat} dt}{C} \tag{1}$$

Where C is the rated battery capacity, for the present case, it is 100Ah. The SOC_{ini} is used to identify the open-circuit voltage (OCV) of the battery (Figure 4).

To accurately characterize the electrochemical behavior of the battery, the open-circuit voltage (OCV) was measured at different states of charge (SOC) as shown in Figure 4.

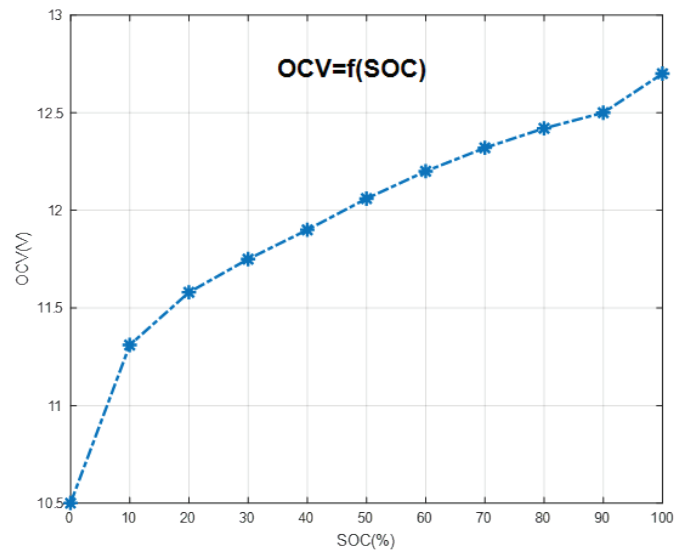


Figure 4: OCV vs SOC curve.

To obtain a curve of OCV as a function of SOC with sufficient resolution to be used correctly in the electrical model, an interval of measurements at 10% of SOC is used. This OCV-SOC curve provides essential information for calibrating the electrical equivalent circuit model and assessing battery

performance under varying charging conditions.

With the lead acid battery operating at a charge rate of C/10 under standard conditions (SOC=50% and T=25°C), as seen in Figure 5, an estimate of the electrical equivalent model parameters was made.

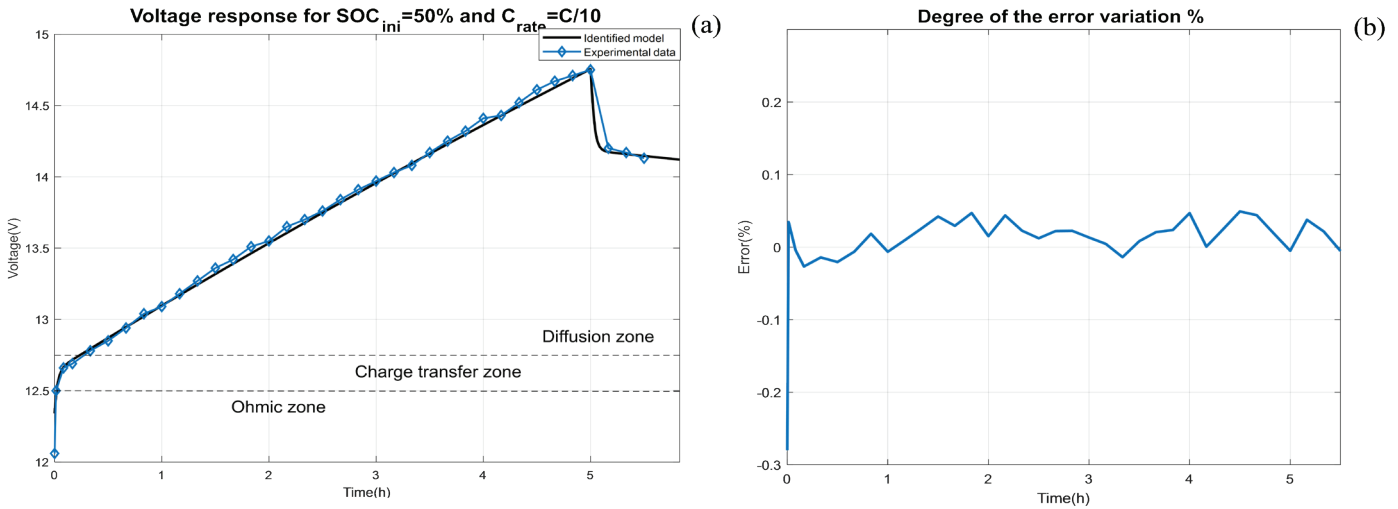


Figure 5: (a) Voltage responses of solar battery with $SOC_{ini}=50\%$ and $C_{rate}=C/10$, (b) battery voltage error.

Table 2 displays the results of parameter identification. In [34], the details of determining the model’s electrical parameters are discussed.

Table 2: Estimated electrical equivalent circuit parameters of the lead acid battery for SOC =50%

Parameters	E_{cq} (V)	R_{Ω} (Ω)	R_{ic} (Ω)	C_{dl} (F)	K_1	K_2
Value	12.06	0.028	0.03	330	6.4510^2	9.5610^{-3}

The comparison between the simulated model voltage response and the experimental voltage response shows that there is no overall divergence between both responses and the total error band is <0.1% (Fig 5 (b)).

B. Evaluation of battery behavior under Various charging profiles

The earlier section presented an evaluation of the primary failure mechanisms in lead batteries, detailing their causes and consequences, based on FMEA tools. Among the causes mentioned, the charging profile is the primary determinant of battery performance, longevity, and reliability. Using the wrong charging profile can facilitate the appearance of the degradation modes and accelerate damage to the battery. Building on the electrical equivalent model presented in the previous section, this section performs an in-depth evaluation of various charging profiles to assess energy efficiency and their impact on battery behavior. The simulation of the different charging profiles, including (a) CC, (b) CC-CV, (c) CC-CV-CC, and (d) PC, is developed and shown in Figure 6.

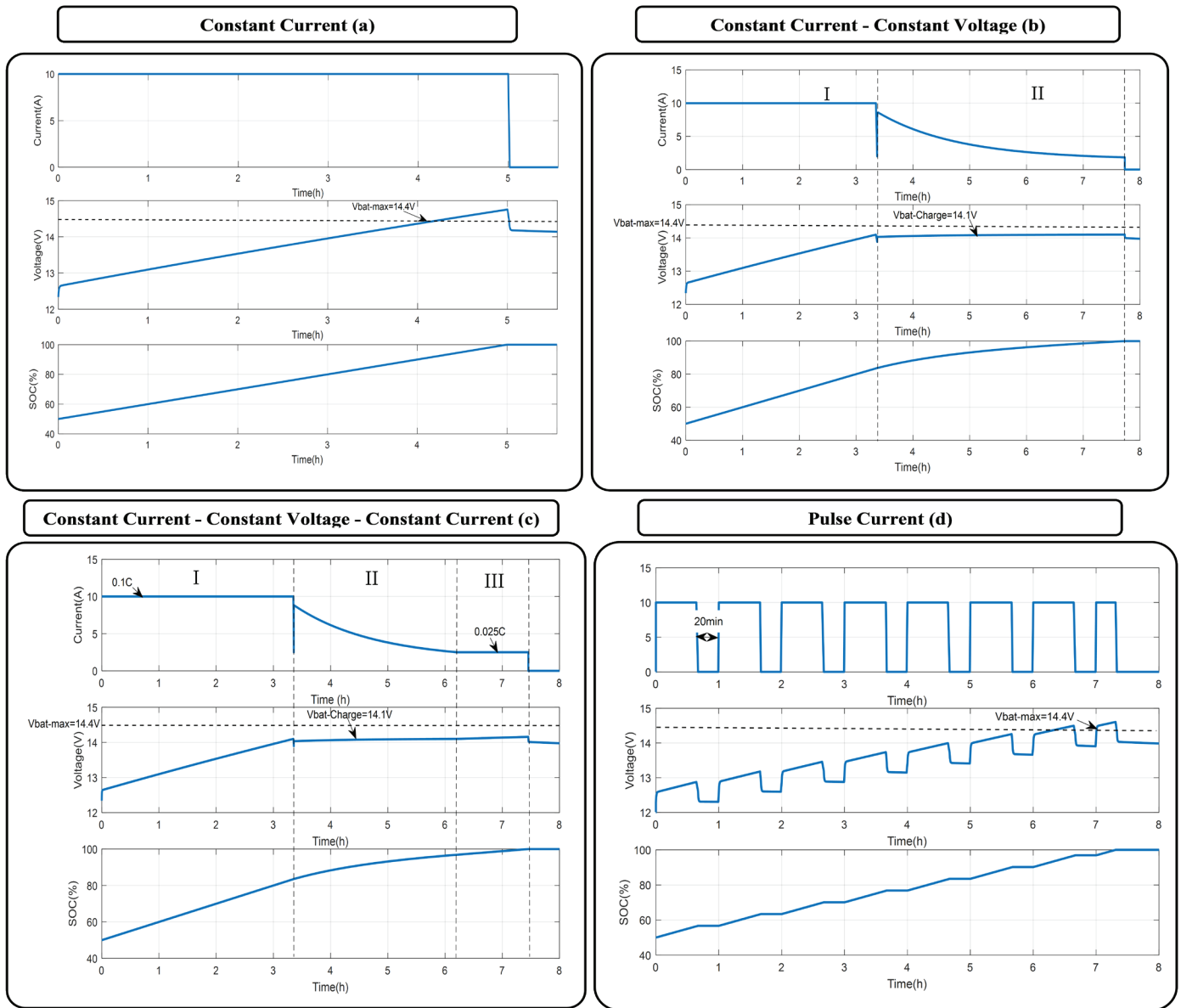


Figure 6: Different charge current profiles for a solar battery.

- Constant Current:** The most commonly used profile to charge the battery is the CC profile (Figure 6.a) due to its ease of programming and its rapidity. Two strategies control the CC profile: charging stops at 100%SOC in the SOC-based method, or at the maximum voltage in the voltage-based method [1]. In this study, the SOC-based method is used. Under a CC charging profile, the duration of charge is directly linked to the current rate, enabling a simple and reliable estimation of charging time. As shown in Figure 6. a, the charging time is 5h with a C-rate equal to C/10 for a battery of 100Ah and SOCini= 50%. The possibility of over-charging and battery temperature rise is a disadvantage of this method, especially when the charge control is based on SOC [9]. As

the result shows, when SOC reaches 100%, the voltage exceeds the maximum voltage (14.4V), which is called the gassing voltage. The gassing voltages indicate when gas formation starts to significantly increase the battery voltage, with the gas current nearing the maximum effective charging current. So, an intense evolution of oxygen gas at the positive plates and hydrogen gas at the negative plates starts. The diffusion phenomena associated with the release of HSO₄⁻ ions in the electrolyte develop polarization overvoltage, which is added to the overvoltage of Ohmic origin. In addition, the crystal formed at active sites will become larger at the end of the charging by constant current, leading to a lower surface area of the active mass [35]. Therefore, the

CC charging profile leads to accelerated aging from overcharging and gas formation, limiting its suitability for high-speed charging in RE applications [36].

- Constant Current - Constant Voltage:** CC-CV charging profile is a common charging profile used for batteries in RE applications (Figure 6.b). This charging profile consists of the combined CC and CV methods. During the CC step, a current of $C/10$ is applied until the battery voltage attains 14.1V. At the beginning of the charging process, the voltage increases while gas generation stays at a low level and does not influence the overall charging behavior. This step is typically used to charge the battery quickly and efficiently. When the charging voltage is attained, the system switches to the CV step (II). Generally, the applied terminal voltage ranges between 2.30V and 2.45 V per cell. This step is used to ensure that the battery is fully charged without overcharging it, which damages the battery. Otherwise, the gassing voltage values depend on both charge reaction rates and gassing reactions. Therefore, gassing voltage values vary with many parameters such as temperature, charge rate, alloy quality, age, and history of the battery. With aging, reduced charge acceptance causes gas evolution to appear earlier during charging. This behavior can lead to increased gas generation and accelerated battery degradation. Another issue with this profile is that the charging time depends on the current rate. Figure 6 illustrates that the charging time with the CC-CV profile is around 7h44min when the battery was supplied with a C-rate equal to $C/10$, which is significantly longer compared to the CC profile. Moreover, continuous charging at currents above $C/10$ promotes temperature rise and can lead to thermal runaway [11]. In the CC-CV charging profile, current selection remains critical, as high currents raise thermal stress while low currents extend the charging duration.
- Constant Current - Constant Voltage - Constant Current:** The third most commonly used profile for charging the battery is a three-step profile, which (Figure 6.c): CC(I)-CV (II)-CC(III). Steps I and III both operate under constant current (or constant power), but step I charges the battery (60-90% of SOC), while step II, called the destratification

phase, is essentially dedicated to the gassing phenomenon. In the second step (II), the charger maintains a constant voltage while the battery's current gradually decreases. This step is used to charge the battery to its full capacity. In step III, the recommended current $C/40$ is applied, exceeding the battery's charge acceptance. This induces gas formation, which helps to homogenize the concentration of the electrolyte in the inter-electrode volume. Otherwise, careful control of energy in the destratification phase is necessary to prevent electrode damage, electrolyte loss, hydrogen hazards, and to ensure efficient energy utilization (e.g., in the case of RE applications, to use the available solar power as efficiently as possible). Therefore, the charge acceptance, like gassing voltage values and gassing current, varies with many parameters such as temperature, charge rate, and age of the battery. During the destratification phase, currents below the battery's charge acceptance do not promote gassing and only delay charging. When the applied current exceeds $C/40$, the uncertainty in charge acceptance and gazing current complicates control, potentially leading to excessive gas evolution and battery degradation. The charging time with the CC-CV-CC profile is around 7h27min, where the destratification phase is around 1h13min. This charging time is shorter than for the CC-CV profile but still longer than the CC profile.

- Pulse Current:** A PC profile for a battery is a charging method that involves the charging mode in short pulses instead of a continuous charge. High current pulses are applied with intermittent rest periods to allow cooling, repeating until full charge is achieved, as shown in Fig 6.d. During the rest periods, the gassing is stopped and allowed for the water and the acid to diffuse into the interior of the plates. This period enables the reaction of the acid with the remainder of the lead oxide in the plates. When the charge current is again started, more lead sulfate is generated, and the water is presented as part of the filling reaction. The rest intervals also permit completion of chemical reactions, thereby helping to prevent excessive gas evolution. This profile is useful not only in providing a time to penetration of the electrolyte but also in decreasing the heat dissipated by the rest period. In the PC profile, the amplitude, duration, and frequency of the

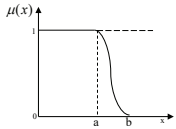
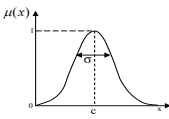
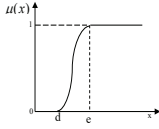
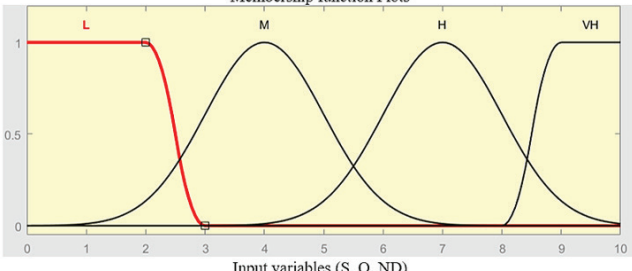
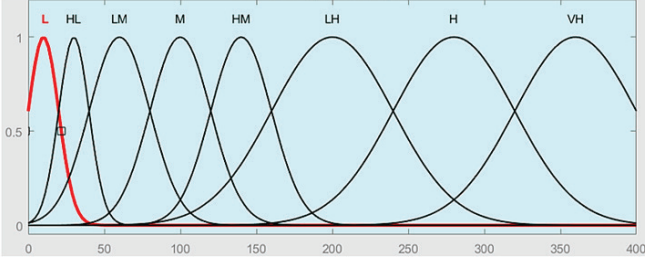
pulses are key parameters that significantly influence the charging behavior [22]. Using a high-frequency PC profile can recover highly sulfated lead-acid batteries and reduce the gas evolution [10]. Thus, in RE applications where batteries may remain partially discharged for extended periods, using a PC profile may increase their operational longevity by reducing the evolution of the lead sulfate on the electrodes, or will even recover the “rechargeability” of those batteries. With high pulsed current charging, the average voltage is similar, but the instantaneous voltage is much higher. This increased driving force allows crystals to form more randomly and rapidly. During the rest periods, the crystal growth will cease. When current is reapplied, new forms rather than existing ones grow further,

preventing excessive crystal enlargement and preserving capacity [36]. To avoid overheating, the pulse duration should be limited so that the temperature rise remains within safe limits. Therefore, the strategy was to keep the pulses with small profiles, i.e., short time at these high voltage levels. As shown in Fig. 6.d, the charging time with PC profile is 7h19min when a current rate of C/10 with a 20 min rest period was applied to the battery, which is longer than the CC profile.

C. Fuzzy FMECA method

For the FRPN assessment in fuzzy FMECA, the input factors “S”, “O”, and “ND” are assigned linguistic levels: Low “L”, Moderate “M”, High “H”, and Very High “VH” (Table 3) [33,34].

Table 3: Ranking and membership functions for input and FRPN factors

Factors	Membership functions		
	Z-Shaped fuzzy membership	Gaussian Fuzzy membership	Z-Shaped fuzzy membership
	 $\mu(x) = \begin{cases} 1, & x \leq a \\ 1 - 2\left(\frac{x-a}{b-a}\right)^2, & a \leq x \leq \frac{a+b}{2} \\ 2\left(\frac{x-b}{b-a}\right)^2, & \frac{a+b}{2} \leq x \leq b \\ 0, & x \geq b \end{cases} \quad (2)$	 $\mu(x) = e^{-\frac{(x-c)^2}{2\sigma^2}} \quad (3)$	 $\mu(x) = \begin{cases} 0, & x \leq d \\ 2\left(\frac{x-d}{e-d}\right)^2, & d \leq x \leq \frac{d+e}{2} \\ 1 - 2\left(\frac{x-e}{e-d}\right)^2, & \frac{d+e}{2} \leq x \leq e \\ 1, & x \geq e \end{cases} \quad (4)$
S, O, ND	<p style="text-align: center;">Membership function Plots</p>  <p style="text-align: center;">Input variables (S, O, ND)</p> <p style="text-align: center;">Low “L”, Moderate “M”, High “H”, and Very High “VH”</p>		
FRPN	<p style="text-align: center;">Membership function Plots</p>  <p style="text-align: center;">Output variables (FRPN)</p> <p style="text-align: center;">Low “L”, High Low “HL”, Low Moderate “LM”, Moderate “M”, High Moderate “HM”, Low High “LH”, High “H”, and Very High “VH”</p>		

The fuzzification of these inputs is implemented in MATLAB using a combination of Gaussian, Z-Shaped, and S-Shaped membership functions. The resulting FRPN is defined over a range from 1 to 1000, classified into 8 ascending levels from Low to Very High (Low “L”, High Low “HL”, Low Moderate “LM”, Moderate “M”, High Moderate “HM”, Low High

“LH”, High “H” and Very High “VH”), modeled using Gaussian membership function. In fuzzy FMECA, the rule base size is given by multiplying the linguistic levels of S, O, and ND [39]. For this study, 64 rules are generated from the three inputs, each with four linguistic terms, as shown in Table 4.

Table 4: The rules in each consequence

				ND			
				Low	Moderate	High	Very high
O	Low	S	Low	L	L	L	L
			Moderate	L	L	L	L
			High	L	L	HL	HL
			Very high	L	HL	HL	LM
	Moderate	S	Low	L	L	L	L
			Moderate	L	HL	LM	LM
			High	HL	LM	M	M
			Very high	LM	M	HM	LH
	High	S	Low	L	L	HL	HL
			Moderate	HL	LM	M	M
			High	LM	M	HM	LH
			Very high	M	HM	LH	H
	Very high	S	Low	L	HL	HL	LM
			Moderate	LM	M	HM	LH
			High	LM	HM	LH	H
			Very high	M	LH	H	VH

Using MATLAB’s Fuzzy Rule Viewer, the impact of membership function shapes on the FRPN output can be analyzed. Adjusting the inputs S, O, and ND allows visualization of both individual rule

responses and the final defuzzified FRPN value [39]. The overall fuzzy inference procedure used to obtain the FRPN value is illustrated in Fig. 7.

Fuzzy FRPN Evaluation Methode Using MATLAB

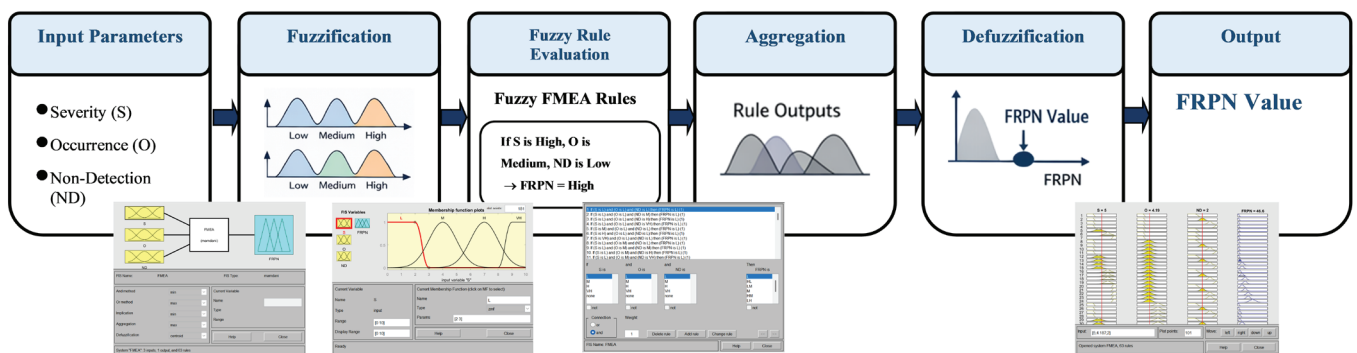


Figure 7: Fuzzy FRPN evaluation procedure using MATLAB.

D. Comparative evaluation of charging profiles

In RE applications, the appropriate charge current profile should strike a compromise between charging time and reliability. Since the effect of charge profiles on battery reliability is a complex topic, a fuzzy risk

assessment was conducted for the various charge current profiles. Table 5 summarizes the total FRPN values and the corresponding charging times for each charging current profile, allowing a comprehensive comparison of their impact on battery degradation and charging performance.

Table 5: Failure risk index evaluation using Fuzzy FMECA and charging time for each profile

Failure modes	Causes	CC profile				CC-CV profile				CC-CV-CC profile				PC profile			
		S ₁	ND ₁	O ₁	FRPN ₁	S ₂	ND ₂	O ₂	FRPN ₂	S ₃	ND ₃	O ₃	FRPN ₃	S ₄	ND ₄	O ₄	FRPN ₄
F1	C1	4	1	4	12.4	4	1	4	12.4	4	1	4	12.4	4	1	4	12.4
	C2	4	1	4	12.4	4	1	4	12.4	1	1	1	12.2	4	1	4	12.4
F2	C3	7	2	1	15.2	7	2	1	15.2	7	2	1	12.4	7	2	1	12.4
	C4	7	1	10	60.1	7	1	4	30.2	7	1	4	30.2	7	1	7	60.1
	C5	7	1	10	60.1	7	1	4	30.2	7	1	4	30.2	7	1	7	60.1
	C6	7	1	7	60.1	7	1	7	60.1	7	1	7	60.1	7	1	7	60.1
F3	C1	7	1	4	30.2	7	1	4	30.2	7	1	4	30.2	4	1	4	12.4
	C2	7	1	4	30.2	7	1	4	30.2	7	1	1	12.3	4	1	4	12.4
F4	C3	10	2	1	30.3	10	2	1	30.3	10	2	1	30.3	10	2	1	30.3
	C5	10	1	10	100	10	1	4	60.1	10	1	4	60.1	10	1	7	60.1
	C4	10	1	10	100	10	1	4	60.1	10	1	4	60.1	10	1	7	60.1
	C1	10	1	4	60.1	10	1	4	60.1	10	1	4	60.1	10	1	4	60.1
	C6	10	3	7	200	10	3	7	200	10	3	7	200	10	3	7	200
	C7	10	3	7	200	10	3	7	200	10	3	7	200	10	3	7	200
Total FRPN		971.1				831.5				810.6				852.9			
Tch		5h				7h44min				7h27min				7h19min			

The evaluation of the failure risk index for each charging profile is performed using the fuzzy FMECA approach. For each failure mode F_i , the FRPN is calculated by summing the FRPN values of its underlying causes C_j :

$$FRPN_{F_i} = \sum_j FRPN_{C_j} \tag{5}$$

For instance, for failure mode F_1 with causes C_1 and C_2 :

$$FRPN_{F_1} = FRPN_{C_1} + FRPN_{C_2} \tag{6}$$

Similarly, for failure mode F_2 with causes C_3 , C_4 , C_5 and C_6 :

$$FRPN_{F_2} = FRPN_{C_3} + FRPN_{C_4} + FRPN_{C_5} + FRPN_{C_6} \tag{7}$$

The total FRPN for each charging profile is then obtained by summing the FRPN_s of all failure modes:

$$FRPN_{total,profile} = \sum_i FRPN_{F_i} \tag{8}$$

This procedure allows the quantitative assessment of risk for each charging profile, taking into account both the individual causes and the failure modes, as reported in Table 5 alongside the corresponding charging times 'Tch'.

As can be seen in Table 5, the main aging mode of the batteries in RE applications is F4 (the non-cohesion of the active mass) with a very high severity equal to 10 for all profiles. Then, F2 (the corrosion of the electrode) and F3 (the hard sulfating of the electrode) with a high severity equal to 7, except for the PC profile, where the severity of F3 decreased to 4 due to its ability to recover highly sulfated lead-acid batteries. F1 (the stratification of the electrolyte) has a medium severity equal to 4 for all charge profiles except the CC-CV-CC profile, where the severity of F1 decreased to 1 due to its ability to homogenize the concentration of the electrolyte.

Whatever the type of charge profile, the intensive uses of the battery (C6) and cycling (C7) in RE

applications have a high occurrence probability equal to 7. Another cause of battery aging in RE applications is the deep discharge with the absence of charge (C1), which has a medium occurrence probability equal to 4. To avoid C1, which causes F1, F2, and F4, an energy management system is required by fixing the maximum state of discharging at 40% in the RE applications [29]. The bad operation of the charger (C3) has a low occurrence probability equal to 1, whatever the type of charge profile.

According to the fuzzy risk assessment, the CC profile is the worst charge profile for batteries in RE applications with an FRPN value of 971,1. The main drawbacks of this profile are overcharging (C4) and overheating (C5), with very high occurrence probability. The incomplete charge (C2) has an occurrence value equal to 4 when the charge control of the CC profile is based on the battery's voltage. This facilitates the stratification of electrolyte F1 and the hard sulfating of the electrodes F3. Therefore, the average life of the battery using the CC profile in RE applications is the lowest. The PC profile has a lower FRPN value than the CC profile of about 852,9 as the occurrence of C4 and C5 decreases to 7, and the severity of F3 decreases to 4 when a higher frequency is used. For the profiles CC-CV and CC-CV-CC, the FRPN value is 831.5 and 810.6, respectively, with a medium occurrence probability of C4 and C5. In fact, the gassing voltage value is not fixed and is affected by the age and history of the battery. At the beginning of battery lifetime, C4 and C5 are avoided. As the battery ages, the transient phase decreases and the gassing voltage increases compared to a new battery. For that, F3 and F4 are not the main aging modes when using these charge profiles. The benefit of the CC-CV-CC profile against the CC-CV profile is its efficiency to avoid F1, by the use of low current at the end of charge, so the severity of this aging mechanism is low.

In addition to this reliability assessment, the charging times reported in Table 5 provide an operational perspective: profiles with shorter charging times, such as CC, allow faster energy replenishment, while longer charging profiles, like CC-CV and CC-CV-CC, may reduce system availability despite potentially lower risks. Considering both reliability (FRPN values) and charging time 'Tch', these insights form the basis for a comparative analysis using combined score TOPSIS and Pareto methods to identify the most balanced charging strategy.

To ensure comparability between the criteria, the FRPN and T_{ch} values were first normalized using the min-max normalization method. For a given criterion x_i, the normalized value is calculated as:

$$x_i^{norm} = \frac{x_i - x_{min}}{x_{max} - x_{min}} \tag{9}$$

Based on these normalized indicators, a Combined score was calculated to provide a balanced evaluation of the charging profiles.

$$Score_{combined} = \frac{FRPN_{norm} + T_{ch-norm}}{2} \tag{10}$$

Where $FRPN_{norm}$ represents the normalized reliability indicator, and $T_{ch-norm}$ represents the normalized charging time.

In addition, the TOPSIS method was applied to rank the charging profiles according to their proximity to an ideal solution characterized by minimum FRPN and minimum T_{ch}. The Euclidean distances from the ideal and anti-ideal solutions are calculated as [40, 41]:

$$v_j^+ = [\min(T_{ch}), \min(FRPN)] \tag{11}$$

$$v_j^- = [\max(T_{ch}), \max(FRPN)] \tag{12}$$

With

v_j^+ is the ideal value for each criterion (best T_{ch}, best FRPN)

v_j^- is the anti-ideal value for each criterion (worst T_{ch}, worst FRPN)

$$D_i^+ = \sqrt{\sum_{j=1}^N (v_{ij} - v_j^+)^2} \tag{13}$$

$$D_i^- = \sqrt{\sum_{j=1}^N (v_{ij} - v_j^-)^2} \tag{14}$$

With

D_i^+ = Euclidean distance of the i-th charging profile from the positive ideal solution

D_i^- = Euclidean distance of the i-th charging profile from the anti-ideal solution

v_{ij} = weighted normalized value of the i-th charging profile for the j-th criterion.

N = Nombre of profiles

The relative closeness to the ideal solution is then obtained as:

$$C_i = \frac{D_i^-}{D_i^+ + D_i^-} \tag{15}$$

In addition, a Pareto analysis was performed to

visualize the trade-off between charging time and reliability. A charging profile is considered Pareto optimal if no other profile improves one criterion without degrading the other. Figure 8 illustrates the results of the comparative assessment of charging profiles using the combined score, TOPSIS, and Pareto analysis based on FRPN and charging time.

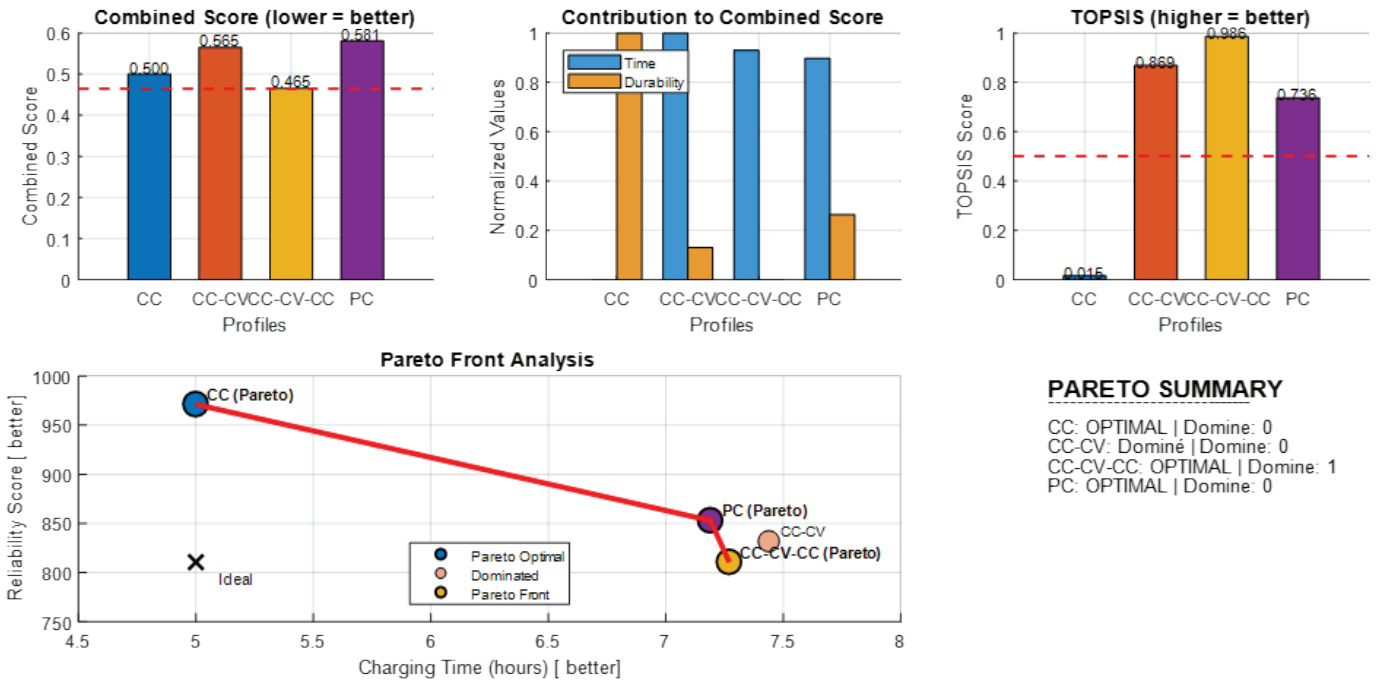


Figure 8: Comparison of charging profiles using the combined score, TOPSIS, and Pareto analysis based on FRPN and charging time.

The results obtained from the Combined score analysis, illustrated in Fig 8, reveal noticeable differences among the considered charging profiles. Since both criteria are to be minimized (shorter charging time and lower FRPN are preferable), a lower Combined Score indicates a more favorable charging profile. The PC profile achieves the highest Combined score (0.581), indicating the least favorable trade-off between charging time and FRPN. The CC-CV profile follows with a score of 0.565, showing competitive performance in balancing both criteria. In contrast, the CC-CV-CC profile presents a slightly lower score (0.465), suggesting a more optimal compromise, while the CC profile obtains a value of approximately 0.500, showing a moderate balance between the two criteria.

The TOPSIS analysis provides further insight into the relative ranking of the charging profiles. As shown in Fig 8, the CC-CV-CC profile achieves the highest TOPSIS score (0.986), indicating the closest proximity to the ideal solution defined by minimum

FRPN and minimum charging time. The PC profile also demonstrates strong performance with a TOPSIS score of 0.736, confirming its balanced characteristics between the two criteria. In contrast, the CC profile shows a very low TOPSIS score (0.015), indicating that although it enables fast charging, its reliability performance makes it significantly distant from the ideal solution.

To further analyze the trade-off between charging time and reliability, a Pareto analysis was conducted. The results presented in Fig 8 show that the PC and CC-CV-CC profiles lie close to the Pareto optimal region, indicating that these profiles offer balanced performance in terms of both criteria. On the other hand, the CC profile appears at the extreme region of minimum charging time but with higher reliability risk, suggesting that the gain in charging speed may come at the expense of increased battery degradation over long-term operation. Overall, the combined use of the combined score evaluation, TOPSIS ranking, and Pareto analysis provides a comprehensive

framework for comparing charging profiles. These complementary methods demonstrate that charging profiles cannot be evaluated solely based on charging time. While the CC profile enables the short charging duration, the combined evaluation of reliability and operational efficiency indicates that profiles such as PC and CC-CV-CC provide a more balanced compromise. These results highlight the importance of integrating reliability indicators such as FRPN with operational parameters when selecting optimal charging strategies for battery energy storage systems.

V. Proposed novel reliability-oriented charging profile

In the previous section, a comprehensive comparison between the various charging profiles in RE applications was carried out based on reliability and charging time coefficients. The analysis shows that the issues related to these charge profiles are overcharging, overheating, incomplete charging, and long charging time. A high charge current

during the initial steps of charging can reduce the charging time, while a gradual decrease towards the end of the charging cycle can ensure the battery is fully charged without overcharging or overheating. In this context, a new charge profile based on three steps is proposed in this section to ensure battery optimal performance and longevity, as shown in Figure 9. In the first step (I), the battery is charged with a high pulse current instead of a continuous current until it reaches the gassing voltage (14.4V). The aim of this step is to reduce the evolution of the lead sulfate (PbSO₄) crystals on the electrodes and charge the battery quickly and efficiently. In the second step (II), the charger switches to the constant voltage “Gassing Voltage” while the battery’s current gradually decreases. This step is used to charge the battery, 60 to 99% of SOC appropriately, and avoid the gassing phenomenon. In the third step (III), the battery is charged with a low constant current until the SOC reach 100%. The aim of this step is to charge the battery to its full capacity and to homogenize the electrolyte concentration in the inter-electrode volume, which can avoid the stratification phenomenon.

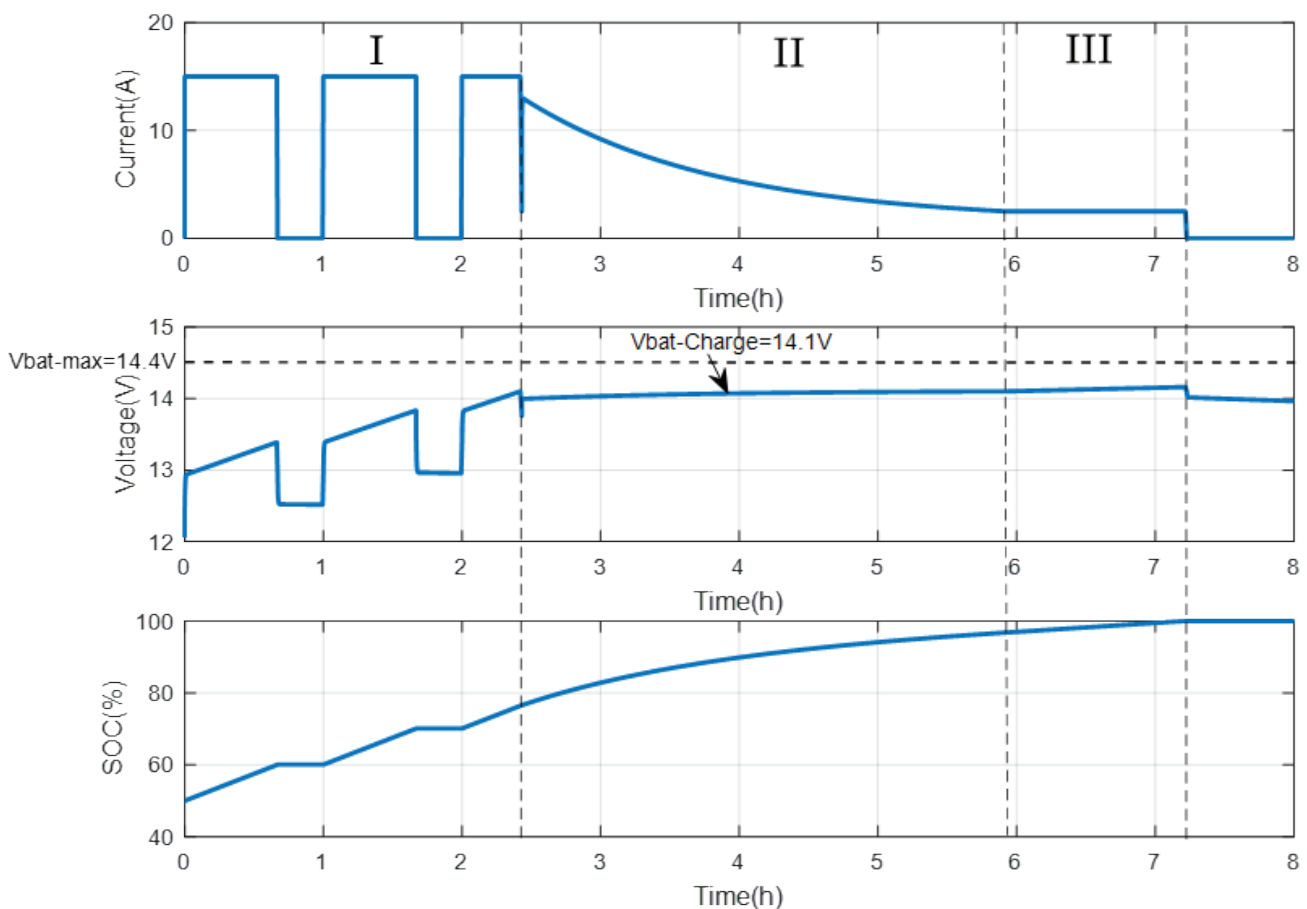


Figure 9: Three-step charging current profile (7h13min).

Table 6 shows the fuzzy risk assessment of the three-step charge current profile and the corresponding charging time.

Table 6: Risk priority number for the three-step current profile and the corresponding charging time

Failure modes	Causes	Three Steps Current profile			
		S	ND	O ₁	FRPN ₁
F1	C1	4	1	4	12.4
	C2	1	1	4	12.2
F2	C3	7	2	1	15.2
	C4	7	1	4	30.2
	C5	7	1	4	30.2
	C6	7	1	7	60.1
F3	C1	4	1	4	12.4
	C2	4	1	4	12.4
F4	C3	10	2	1	30.3
	C5	10	1	4	60.1
	C4	10	1	4	60.1
	C1	10	1	4	60.1
	C6	10	3	7	200
	C7	10	3	7	200
	Total FRPN	795.7			
Tch	7h 13min				

The comparative evaluation of the charging profiles, including the new profile, is presented in Fig 10. The analysis combines three multi-criteria approaches:

combined score, TOPSIS ranking, and Pareto analysis to evaluate the trade-off between battery reliability (FRPN) and charging time.

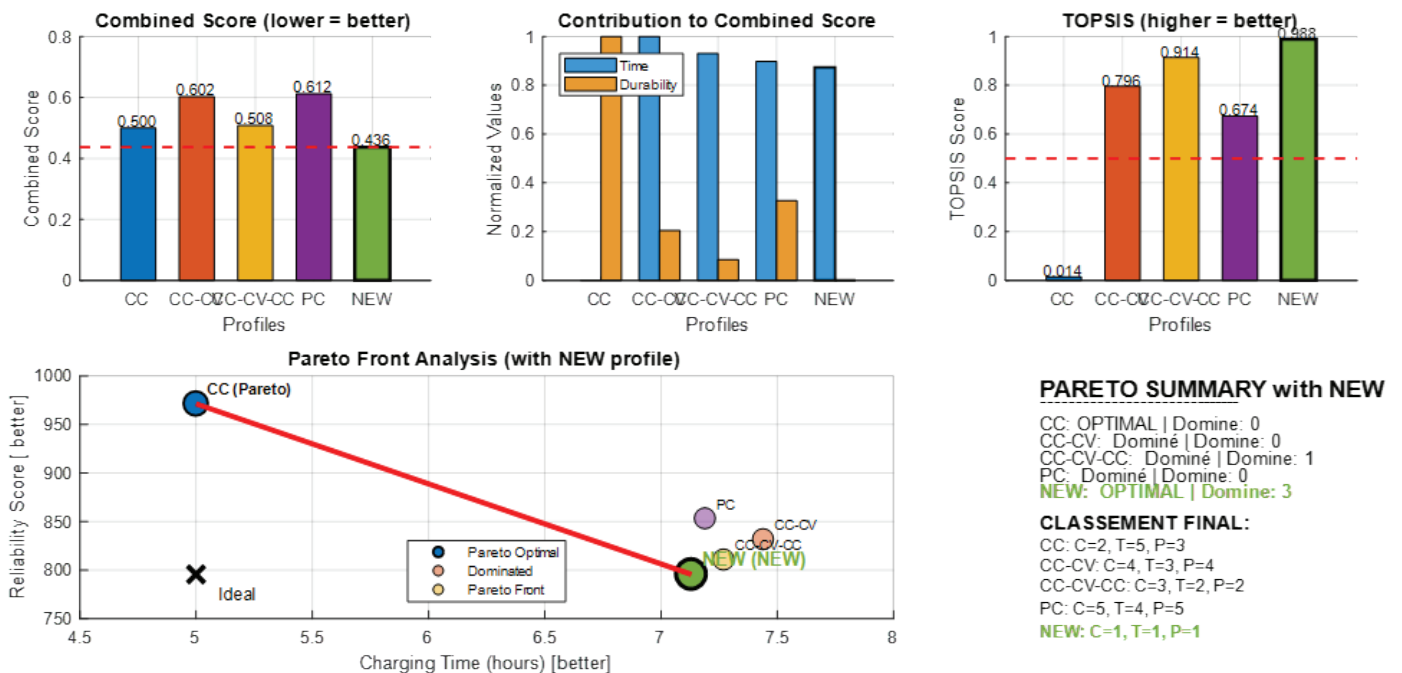


Figure 10: Comparison of conventional and proposed charging profiles using combined score, TOPSIS, and Pareto analysis.

As shown in Figure 10, while the combined score slightly favors the new profile (0.436), the TOPSIS results indicate that the new profile achieves the highest score (0.988), corresponding to the closest proximity to the ideal solution defined by minimum FRPN and minimum charging time. The Pareto analysis further confirms this trend, showing that the new profile lies on the Pareto front and dominates three other profiles, indicating an improved trade-off between charging time and reliability. Overall, the combined analysis suggests that the new charging strategy represents a promising solution for achieving an improved balance between charging efficiency and battery reliability.

VI. Conclusions

Batteries deployed in RE applications are subjected to harsh environments and operating conditions, which encourage the occurrence of several aging modes, including stratification of electrolyte, corrosion of the electrodes, hard sulfating of the electrodes, and poor cohesion of the active mass. To mitigate the aging modes, it is important to use high-quality batteries, maintain them properly, and use the right charge profile. The charge profile can have a significant impact on the battery's performance

and longevity. In this regard, a comprehensive comparison of various charge profiles using the fuzzy method was provided. Seven critical failure causes (C1..., C7) were identified through the analysis of the various aging mechanisms of the solar battery using the FMEA technique.

The results obtained using fuzzy logic analysis showed that the selected profile allowing the improvement of the solar batteries' performances is the CC-CV-CC profile, with an FRPN value of 810.6 and a charging time Tch of 7h 17min, achieving a Combined score of 0.465 and a TOPSIS score of 0.986. This charging profile has a better compromise between reliability (FRPN) and charging time among the other profiles. Otherwise, CC, CC-CV, and PC profiles show moderate efficiency, with Combined scores of 0.500, 0.565, and 0.581, respectively.

This study is completed by elaborating a new charging profile based on a combination of PC and CC-CV-CC profiles. The proposed new profile achieves a TOPSIS score of 0.988, lies on the Pareto front, and dominates 4 other profiles, demonstrating a highly efficient trade-off between charging time Tch and reliability (FRPN). This strategy allows a significant improvement in the expected life and performance of batteries dedicated to RE applications.

References

- [1] R. Yahmadi, K. Brik, and F. Ben Ammar, "Improvement of energy management system for maximum battery reliability in standalone photovoltaic applications," *Journal of Electrical Engineering*, vol. 18, no. 2, pp. 81-91, 2018.
- [2] W. Jing, C. H. Lai, D. K. X. Ling, W. S. H. Wong, and M. L. D. Wong, "Battery lifetime enhancement via smart hybrid energy storage plug-in module in standalone photovoltaic power system," *Journal of Energy Storage*, vol. 21, pp. 586-598, Feb. 2019, doi: <https://doi.org/10.1016/j.est.2018.12.007>.
- [3] M. T. Yeshalem and B. Khan, "Design of an off-grid hybrid PV/wind power system for remote mobile base station: A case study," *AIMS Energy*, vol. 5, no. 1, pp. 96-112, 2017, doi: <https://doi.org/10.3934/energy.2017.1.96>.
- [4] R. Yahmadi, K. Brik, and F. Ben Ammar, "Research of critical causes and improvement of energy storage system reliability in power electronic applications," *International Journal of Hydrogen Energy*, vol. 42, no. 13, pp. 8765-8776, Mar. 2017, doi: <https://doi.org/10.1016/j.ijhydene.2016.10.034>.
- [5] R. Yahmadi, K. Brik, and F. ben Ammar, "Fuzzy risk priority number assessment for solar gel battery manufacturing defects," *Engineering Failure Analysis*, vol. 124, 2021, doi: <https://doi.org/10.1016/j.engfailanal.2021.105327>.
- [6] J. Balaraju, M. Govinda Raj, and C. S. Murthy, "Fuzzy-FMEA risk evaluation approach for LHD machine-A case study," *Journal of Sustainable Mining*, vol. 18, no. 4, pp. 257-268, Nov. 2019, doi: <https://doi.org/10.1016/j.jsm.2019.08.002>.

- [7] E. Freeman, D. Occello, and F. Barnes, "Energy storage for electrical systems in the USA," *AIMS Energy*, vol. 4, no. 6, pp. 856–875, 2016, doi: <https://doi.org/10.3934/energy.2016.6.856>.
- [8] A. M. S. M. H. S. Attanayaka, J. P. Karunadasa, and K. T. M. U. Hemapala, "Estimation of state of charge for lithium-ion batteries - A Review," *AIMS Energy*, vol. 7, no. 2, pp. 186–210, 2019, doi: <https://doi.org/10.3934/energy.2019.2.186>.
- [9] H. Bizhani, S. Kamal, H. Rezazadeh, and S. Muyeen, "A Comprehensive Comparison of a Lead-Acid Battery Electro-Thermal Performance Considering Different Charging Profiles," *2021 IEEE 4th International Conference on Computing, Power and Communication Technologies (GUCON)*, Sep. 2021, doi: <https://doi.org/10.1109/gucon50781.2021.9573724>.
- [10] M. James, J. Grummett, M. Rowan, and J. Newman, "Application of pulse charging techniques to submarine lead-acid batteries," *Journal of Power Sources*, vol. 162, no. 2, pp. 878–883, Nov. 2006, doi: <https://doi.org/10.1016/j.jpowsour.2005.02.018>.
- [11] S. Lavety, R. K. Keshri, and M. A. Chaudhari, "Evaluation of Charging Strategies for Valve Regulated Lead-Acid Battery," *IEEE Access*, vol. 8, pp. 164747–164761, 2020, doi: <https://doi.org/10.1109/access.2020.3022235>.
- [12] R. K. Sharma, D. Kumar, and P. Kumar, "Systematic failure mode effect analysis (FMEA) using fuzzy linguistic modelling," *International Journal of Quality & Reliability Management*, vol. 22, no. 9, pp. 986–1004, Dec. 2005, doi: <https://doi.org/10.1108/02656710510625248>.
- [13] R. R. Elbanna, M. H. ElMessmary, H. Diab, and M. Abdelsalam, "A smart hybrid optimization model for DSSE in renewable energy-powered distribution networks," *Renewable Energy and Sustainable Development*, vol. 11, no. 2, p. 314, Sep. 2025, doi: <https://doi.org/10.21622/resd.2025.11.2.1271>.
- [14] P. S. Kumar, C. Chandrika, P. K. Rao, P. K. Rao, and S. K. Oruganti, "Interpretable hybrid machine learning models for renewable-powered smart grid stability prediction," *Renewable Energy and Sustainable Development*, vol. 11, no. 2, p. 397, Oct. 2025, doi: <https://doi.org/10.21622/resd.2025.11.2.1509>.
- [15] R. Yahmadi, K. Brik, and F. Ben Ammar, "Sizing and improving performances of a photovoltaic water pumping system for irrigation in Jerid Tunisia," *2019 10th International Renewable Energy Congress (IREC)*, pp. 1–6, Mar. 2019, doi: <https://doi.org/10.1109/irec.2019.8754534>.
- [16] S. Boral, I. Howard, S. K. Chaturvedi, K. McKee, and V. N. A. Naikan, "An integrated approach for fuzzy failure modes and effects analysis using fuzzy AHP and fuzzy MAIRCA," *Engineering Failure Analysis*, vol. 108, p. 104195, Jan. 2020, doi: <https://doi.org/10.1016/j.engfailanal.2019.104195>.
- [17] W. Song, X. Ming, Z. Wu, and B. Zhu, "A rough TOPSIS Approach for Failure Mode and Effects Analysis in Uncertain Environments," *Quality and Reliability Engineering International*, vol. 30, no. 4, pp. 473–486, Feb. 2013, doi: <https://doi.org/10.1002/qre.1500>.
- [18] A. A. Supciller and N. Abali, "Occupational Health and Safety Within the Scope of Risk Analysis with Fuzzy Proportional Risk Assessment Technique (Fuzzy Prat)," *Quality and Reliability Engineering International*, vol. 31, no. 7, pp. 1137–1150, Oct. 2015, doi: <https://doi.org/10.1002/qre.1908>.
- [19] G. Di Bona, A. Silvestri, A. Forcina, and A. Petrillo, "Total efficient risk priority number (TERPN): a new method for risk assessment," *Journal of Risk Research*, vol. 21, no. 11, pp. 1384–1408, Apr. 2017, doi: <https://doi.org/10.1080/13669877.2017.1307260>.
- [20] N. G. Mutlu and S. Altuntas, "Risk analysis for occupational safety and health in the textile industry: Integration of FMEA, FTA, and BIFPET methods," *International Journal of Industrial Ergonomics*, vol. 72, pp. 222–240, Jul. 2019, doi: <https://doi.org/10.1016/j.ergon.2019.05.013>.
- [21] C.-F. Chi, D. Sigmund, and M. O. Astaridi, "Classification Scheme for Root Cause and Failure Modes and Effects Analysis (FMEA) of Passenger Vehicle Recalls," *Reliability Engineering & System Safety*, p. 106929, Mar. 2020, doi: <https://doi.org/10.1016/j.res.2020.106929>.

- [22] K. Jenab, R. M. Blecher, and S. Moslehpour, "SRB Field Joints Failure Analysis Using Fuzzy FMEA," *International Journal of Physics and Astronomy*, vol. 3, no. 1, 2015, doi: <https://doi.org/10.15640/ijpa.v3n1a1>.
- [23] H.-C. Liu, X. Fan, P. Li, and Y. Chen, "Evaluating the risk of failure modes with extended MULTIMOORA method under fuzzy environment," *Engineering Applications of Artificial Intelligence*, vol. 34, pp. 168–177, Sep. 2014, doi: <https://doi.org/10.1016/j.engappai.2014.04.011>.
- [24] F. Tamtam and A. Tourabi, "Innovative fuzzy VIKOR approach for green hydrogen technologies assessment: implications for sustainable energy development," *Renewable Energy and Sustainable Development*, vol. 11, no. 2, p. 229, Aug. 2025, doi: <https://doi.org/10.21622/resd.2025.11.2.1283>.
- [25] R. T. Moyo, M. Dewa, H. F. M. Romero, V. A. Gómez, J. I. M. Aragonés, and L. Hernández-Callejo, "An adaptive neuro-fuzzy inference scheme for defect detection and classification of solar PV cells," *Renewable Energy and Sustainable Development*, vol. 10, no. 2, p. 218, Sep. 2024, doi: <https://doi.org/10.21622/resd.2024.10.2.929>.
- [26] M. Kumru and P. Y. Kumru, "Fuzzy FMEA application to improve purchasing process in a public hospital," *Applied Soft Computing*, vol. 13, no. 1, pp. 721–733, Jan. 2013, doi: <https://doi.org/10.1016/j.asoc.2012.08.007>.
- [27] M. Braglia, M. Frosolini, and R. Montanari, "Fuzzy criticality assessment model for failure modes and effects analysis," *International Journal of Quality & Reliability Management*, vol. 20, no. 4, pp. 503–524, Jun. 2003, doi: <https://doi.org/10.1108/02656710310468687>.
- [28] H. Shirouyehzad, M. Badakhshian, R. Dabestani, and H. Panjehfouladgaran, "Fuzzy FMEA Analysis For Identification And Control Of Failure Preferences In ERP Implementation," *Journal of Mathematics and Computer Science*, vol. 01, no. 04, pp. 366–376, Dec. 2010, doi: <https://doi.org/10.22436/jmcs.001.04.14>.
- [29] S. Vinodh, S. Aravindraj, R. Sathya Narayanan, and N. Yogeshwaran, "Fuzzy assessment of FMEA for rotary switches: a case study," *The TQM Journal*, vol. 24, no. 5, pp. 461–475, Aug. 2012, doi: <https://doi.org/10.1108/17542731211261601>.
- [30] L. Song and J. W. Evans, "Electrochemical-Thermal Model of Lithium Polymer Batteries," *Journal of The Electrochemical Society*, vol. 147, no. 6, pp. 2086–2095, 2000, doi: <https://doi.org/10.1149/1.1393490>.
- [31] M. Chen and G. A. Rincon-Mora, "Accurate Electrical Battery Model Capable of Predicting Runtime and I-V Performance," *IEEE Transactions on Energy Conversion*, vol. 21, no. 2, pp. 504–511, Jun. 2006, doi: <https://doi.org/10.1109/tec.2006.874229>.
- [32] R. Islam, S.-Y. Park, and B. Balasingam, "Unification of Internal Resistance Estimation Methods for Li-Ion Batteries Using Hysteresis-Free Equivalent Circuit Models," *Batteries*, vol. 6, no. 2, p. 32, Jun. 2020, doi: <https://doi.org/10.3390/batteries6020032>.
- [33] K. Brik and F. ben Ammar, "Causal tree analysis of depth degradation of the lead acid battery," *Journal of Power Sources*, vol. 228, pp. 39–46, Apr. 2013, doi: <https://doi.org/10.1016/j.jpowsour.2012.10.088>.
- [34] S. Madani, E. Schaltz, and S. Knudsen Kær, "An Electrical Equivalent Circuit Model of a Lithium Titanate Oxide Battery," *Batteries*, vol. 5, no. 1, p. 31, Mar. 2019, doi: <https://doi.org/10.3390/batteries5010031>.
- [35] Y. Yu *et al.*, "Constructing Accurate Equivalent Electrical Circuit Models of Lithium Iron Phosphate and Lead-Acid Battery Cells for Solar Home System Applications," *Energies*, vol. 11, no. 9, p. 2305, Sep. 2018, doi: <https://doi.org/10.3390/en11092305>.
- [36] R. Yahmadi, K. Brik, and F. ben Ammar, "Causal tree analysis for quality control of the lead acid battery manufacturing process," *International Journal of Energy Research*, vol. 42, no. 4, pp. 1738–1759, Jan. 2018, doi: <https://doi.org/10.1002/er.3987>.

- [37] R. Yahmadi, K. Brik, and F. Ammar, "Analysis Approach of the Formation Current Profiles Impact on the Lead Acid Battery Manufacturing," *Recent Advances in Electrical & Electronic Engineering (Formerly Recent Patents on Electrical & Electronic Engineering)*, vol. 9, no. 3, pp. 231–240, Feb. 2017, doi: <https://doi.org/10.2174/2352096509666161110105048>.
- [38] M. James, J. Grummett, M. Rowan, and J. Newman, "Application of pulse charging techniques to submarine lead-acid batteries," *Journal of Power Sources*, vol. 162, no. 2, pp. 878–883, Nov. 2006, doi: <https://doi.org/10.1016/j.jpowsour.2005.02.018>.
- [39] N. Chanamool and T. Naenna, "Fuzzy FMEA application to improve decision-making process in an emergency department," *Applied Soft Computing*, vol. 43, no. 4, pp. 441–453, 2016, doi: <https://doi.org/10.1016/j.asoc.2016.01.007>.
- [40] W. Song, X. Ming, Z. Wu, and B. Zhu, "A rough TOPSIS Approach for Failure Mode and Effects Analysis in Uncertain Environments," *Quality and Reliability Engineering International*, vol. 30, no. 4, pp. 473–486, Feb. 2013, doi: <https://doi.org/10.1002/qre.1500>.
- [41] H. Taherdoost and M. Madanchian, "A Comprehensive Survey and Literature Review on TOPSIS," *International Journal of Service Science, Management, Engineering, and Technology*, vol. 15, no. 1, pp. 1–65, Aug. 2024, doi: <https://doi.org/10.4018/ijssmet.347947>.